Hybrid Dynamic Density Functional Theory for Polymer Melts and Blends

Takashi Honda*

Japan Chemical Innovation Institute, and Department of Organic and Polymeric Materials, Tokyo Institute of Technology, Ookayama, Meguro-ku, Tokyo 152-8552, Japan

Toshihiro Kawakatsu

Department of Physics, Tohoku University, Aoba, Aramaki, Aoba-ku, Sendai 980-8578, Japan

Received September 4, 2006; Revised Manuscript Received December 12, 2006

ABSTRACT: We propose a high-speed and accurate hybrid dynamic density functional theory for the computer simulations of the phase separation processes of polymer melts and blends. The proposed theory is a combination of the dynamic self-consistent-field (SCF) theory and a time-dependent Ginzburg−Landau type theory with the random phase approximation (GRPA). The SCF theory is known to be accurate in evaluating the free energy of the polymer systems in both weak and strong segregation regions although it has a disadvantage of the requirement of a considerable amount of computational cost. On the other hand, the GRPA theory has an advantage of much smaller amount of required computational cost than the SCF theory while its applicability is limited to the weak segregation region. To make the accuracy of the SCF theory and the high-performance of the GRPA theory compatible, we adjust the chemical potential of the GRPA theory by using the SCF theory every constant time steps in the dynamic simulations. The performance of the GRPA and the hybrid theories is tested by using several systems composed of an A/B homopolymer, an AB diblock copolymer, or an ABC triblock copolymer. Using the hybrid theory, we succeeded in reproducing the metastable complex phase-separated domain structures of an ABC triblock copolymer observed by experiments.

1. Introduction

Polymer phase separation is an important problem in the practical applications of polymeric materials composed of polymer alloys, polymer blends, and polymeric additives, etc. These materials show several types of phase separations, i.e., micro- and macrophase separations, and phase separations induced by chemical reactions and external fields. By controlling the morphology of the domains generated by the phase separations, we can design the physical properties of these polymeric materials such as permeability, electrical conductivity, and mechanical properties.[1,2] Therefore, understanding the mechanisms of the phase separation and the domain formation is very important in studying polymeric materials. For this purpose, the density functional theories based on coarse-grained models of the polymer chains have been being used as important techniques.[3−5]

In coarse-grained models of polymers, a polymer chain is modeled as a sequence of segments, which define the smallest length scale of the model.[6] In the density functional theories, the free energy of the system is expressed as a functional of the density distributions of the segments. Using such an expression of the free energy, one can evaluate the chemical potential of each segment density. In a diffusion dynamics, the segment density is driven by the spatial gradient of this chemical potential. Depending on how the free energy is evaluated, the accuracy and the computational cost of the dynamic simulations are determined. The more the accuracy is improved, the more the computational cost is, in general, required. Therefore, it is important to establish a new technique where these two factors, i.e., the accuracy and the computational cost, are improved simultaneously.

* Corresponding author. E-mail: thonda@polymer.titech.ac.jp.

A typical density functional theory that can give an accurate and reliable free energy is the self-consistent-field (SCF) theory.[6−8] In this SCF theory, the free energy and the chemical potential are accurately evaluated by taking account of the conformational entropy of the chains, which is described in terms of path integral technique under mean-field approximation. A dynamic SCF theory is a dynamical extension of this SCF theory, where the diffusion dynamics of the segment densities is assumed.[6,9−12] A simulation of this dynamic SCF theory requires recursive calculations to get the chemical potentials, which requires a considerable amount of computational cost.

There are other types of density functional theories which are based on simple phenomenological models of the free energy functional. Typical examples are the time-dependent Ginzburg−Landau theory and the Flory−Huggins−de Gennes theory.[6,13−19] In most of these theories, an analytical form of the free energy functional is assumed. Using such a model free energy, one can evaluate the chemical potential without using the recursive calculations as is done in the SCF theory. This accelerates the simulations considerably. In this article, we refer these theories as phenomenological density functional (PDF) theories. In most of the PDF theories, the random phase approximation (RPA) plays a very important role.[20,21] With this RPA, one can evaluate both the short-range part and the long-range part of the interaction energies between segment density fluctuations.

The Flory−Huggins−de Gennes PDF theory uses a free energy model where the Flory−Huggins free energy for uniform systems is extended by introducing a square gradient term of the segment density fluctuations derived by the RPA.[13] This theory succeeded to reproduce the spatially inhomogeneous states of the phase separations of blends of linear homopolymers. Leibler obtained a theoretical phase diagram of a diblock copolymer using a power series expansion of the free energy

10.1021/ma0620464 CCC: $37.00 © 2007 American Chemical Society
Published on Web 01/23/2007

up to the fourth-order terms in the segment density fluctuations, where the expansion coefficients are evaluated using the RPA.[22]

Ohta and Kawasaki used a simpler form of the Leibler's free energy by decomposing it into a short-range part and a long-range part and assumed a Ginzburg−Landau (GL) type form for the short-range part while the long-range part is approximated by the long-range asymptotic form of the second-order term in the expansion.[23] They succeeded in reproducing the phase diagram of the microdomain structures of diblock copolymer in the strong segregation region qualitatively.

Contrary to this Ohta−Kawasaki PDF approach using an approximation on the second-order term in the free energy expansion, Bohbot-Raviv and Wang evaluated the second-order term faithfully using the RPA and combined it with the higher-order terms in the expansion of the Flory−Huggins free energy. They predicted several microdomain structures of three-miktoarm star polymers and linear triblock copolymers using static calculations.[24]

Recently, Uneyama and Doi proposed a PDF theory generalizing the Ohta−Kawasaki theory and the Flory−Huggins−de Gennes theory. Uneyama and Doi's model can be used for melts and blends of any types of polymer architectures, i.e., the branching structure and the order of the sequence of the segments along the chain.[25] They could reproduce micellar structures and obtained a phase behavior of the micelles that is in good agreement with the experimental phase diagram.[26] They also applied their theory to dynamic problems associated with phase separations and structural phase transitions.[27]

Despite the success of these static and dynamic PDF theories, there are quantitative discrepancies between the results of the PDF theory and that of the SCF theory. This is because of the truncation error of the Taylor series expansion of the free energy used in the PDF theories. Such a truncation error cannot be negligible from the intermediate to the strong segregation regions. On the other hand, the SCF theory is free from such a truncation error because the SCF theory relies on a numerical evaluation of the path integral, which corresponds to summing up all the terms in the Taylor series expansion of the free energy. Thus, the SCF theory can give accurate results on the phase behavior, as long as the mean-field approximation is valid, even in the strong segregation region where the truncation of the Taylor series expansion used in the PDF theories breaks down.

In refs 28−30, we applied the dynamic SCF theory to dynamics of phase separations and structural phase transitions and evaluated the performance of the dynamic SCF theory. In spite of the accuracy of the dynamic SCF theory, it requires a considerable amount of computational cost compared to the dynamic PDF theories. Thus, a new technique or a new idea is needed to reduce the computational cost of the dynamic SCF theory. The main purpose of the present article is to propose such an idea by combining the dynamic SCF theory and the PDF theory. To realize this idea, the model is constructed according to the following steps.

We first introduce our PDF theory, which will be later combined with the SCF theory. For this purpose, we derive exact expressions of the scattering functions of the segment density fluctuations for polymer melts and blends composed of polymers with any architectures using RPA. Using such scattering functions, we construct the free energy model for our PDF theory where we do not rely on the approximate form of the free energy models proposed by Ohta and Kawasaki and by Uneyama and Doi,[23,25] but we use the more accurate form proposed by Bohbot-Raviv and Wang.[24] As this model is based on the GL free energy whose coefficients are determined using the RPA, we will abbreviate this model as GRPA. Bohbot-Raviv and Wang applied this GRPA theory to static problems such as the equilibrium domain structures. In the present work, we apply this GRPA theory to dynamic problems of polymer melts and blends. We compare the results of the dynamic GRPA theory with those of the other PDF theories.

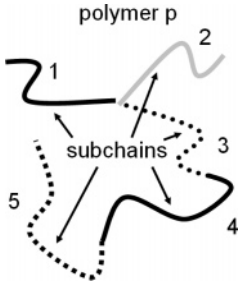

Figure 1. A schematic picture of a polymer architecture treated in this article.

On the basis of the results of the dynamic GRPA theory, we next propose a hybrid theory where the dynamic SCF theory and the dynamic GRPA theory is combined to reduce the computational cost of the dynamic SCF theory without loss of its accuracy. We test this hybrid theory by using several systems as examples. We will show that the hybrid theory considerably accelerates the dynamic SCF theory without spoiling its accuracy. Using this hybrid theory, we investigate the microphase-separation behavior of a linear ABC triblock copolymer, which is known to show many complex domain structures by changing the affinity of the solvent to each of the blocks.[32,33]

For the present study, we used the "Simulation Utilities for Soft and Hard Interfaces (SUSHI)" in the OCTA system.[28]

2. Theory

In this section, we first explain the detail of the static and dynamic GRPA theories. The accuracy of the dynamic GRPA theory is then tested. On the basis of these results, we propose a hybrid dynamic density functional theory that combines the dynamic SCF theory and the dynamic GRPA theory.

We consider a melt or a blend of polymers that have arbitrary molecular architectures. (For simplicity, we assume that the polymers do not have loops.) To construct a coarse-grained model, we adopt the Gaussian chain approximation where the polymers obey the Gaussian statistics on the scale larger than the segment size.[6]

In our model, a polymer chain is divided into subchain(s), each of which is a Gaussian chain composed of the same type of segments. For example, a homopolymer consists of a single subchain and a block copolymer consists of subchains of different kinds. Here, the term "subchains" has the same meaning as a block in a block copolymer. The molecular architecture of a polymer is defined in terms of its branching structures, the sequence of the subchains, the type of the segments that compose each subchain, and the length of each subchain.

We use a superscript index p ($p = 1, 2, 3, ..., m$) to identify the type of the polymer architecture, where m is the total number of polymer types, and a subscript index K to identify the chemical type of the segments. Subscript indices i and j ($i, j = 1, 2, 3, ..., n$) are used to specify the subchains where we denote the number of subchains in a p-type polymer by $n^{(p)}$ and the total number of the subchain types in the system by $n = \sum_p n^{(p)}$. We also define that the number of segments in the ith subchain of a p-type polymer is $N_i^{(p)}$, and the total number of segments of the p-type polymer is $N^{(p)} = \sum_i N_i^{(p)}$.

Figure 1 shows a typical molecular architecture of a polymer chain (a *p*-type chain with $n^p = 5$). Each subchain is specified by the number (i.e., the index $i = 1, 2, ..., n^p$) and the chemical type of each subchain is distinguished using the line style.

We denote the interaction energy between a pair of *K*-type and *K*′-type segments by $\epsilon_{KK'}$. This interaction energy is related to the Flory−Huggins interaction parameter $\chi_{KK'}$ by

$$\chi_{KK'} \equiv z\beta\left\{\epsilon_{KK'} - \frac{1}{2}(\epsilon_{KK} + \epsilon_{K'K'})\right\} \tag{1}$$

where z is the coordination number and $\beta = 1/k_BT$, k_B and T being the Boltzmann constant and the temperature, respectively.

2.1. Ginzburg−Landau Free Energy Based on the Random Phase Approximation. 2.1.1. Free Energy Model of the System. During dynamic simulations, the system has not yet reached its equilibrium state. This means that the segments in different subchains, in general, feel different chemical potentials even if the segments are of the same kind. Thus, the free energy used in the dynamic simulations should be described in terms of the segment density fluctuations of each subchain defined by

$$\delta\phi_i(\mathbf{r}) \equiv \phi_i(\mathbf{r}) - \bar{\phi}_i \tag{2}$$

where $\phi_i(\mathbf{r})$ is the local segment density of the *i*th subchain at position $\mathbf{r}$ and $\bar{\phi}_i$ is the average segment density of the *i*th subchain.

Using the GL expansion that is justified in the weak segregation region, the free energy functional is given by[6]

$$\mathcal{F}[\{\phi_i(\mathbf{r})\}] = \mathcal{F}_0[\{\bar{\phi}_i\}] + \frac{1}{2\beta}\sum_{ij}\int\int d\mathbf{r}\, d\mathbf{r}'\, S_{ij}^{-1}(\mathbf{r}-\mathbf{r}')\,\delta\phi_i(\mathbf{r})\,\delta\phi_j(\mathbf{r}') + ... \tag{3}$$

$$= \mathcal{F}_0[\{\bar{\phi}_i\}] + \frac{1}{2\beta}\sum_{ij}\int d\mathbf{q}\, S_{ij}^{-1}(\mathbf{q})\,\delta\phi_i(\mathbf{q})\,\delta\phi_j(-\mathbf{q}) + ... \tag{4}$$

where the first term $\mathcal{F}_0[\{\bar{\phi}_i\}]$ is the free energy of the uniformly mixed state that is used as the reference state for the expansion. Equations 3 and 4 are the Taylor series expansions of the free energy with respect to the local segment density fluctuations of the subchains. The expansion coefficients, $S_{ij}^{-1}(\mathbf{r}-\mathbf{r}')$, in eq 3 is the inverse of the density−density autocorrelation function between the segment density fluctuations belonging to the *i*th and *j*th subchains at positions $\mathbf{r}$ and $\mathbf{r}'$, respectively. Its Fourier representation is $S_{ij}^{-1}(\mathbf{q})$ in eq 4, where $\mathbf{q}$ is the scattering wave vector. The dots at the ends of eqs 3 and 4 mean the higher-order terms in the Taylor series expansion in $\delta\phi_i(\mathbf{r})$ or $\delta\phi_i(\mathbf{q})$, respectively.

Using this GL expansion, Bohbot-Raviv and Wang tried to include the effects of the spatial inhomogeneity into the Flory−Huggins free energy for uniform systems. They replaced the second-order contributions in $\delta\phi_i(\mathbf{r})$ in the Flory−Huggins free energy with the second term of eq 4, and they obtained the following expression:[24]

$$\mathcal{F}[\{\phi_i(\mathbf{r})\}] = \frac{1}{\beta}\sum_i\int d\mathbf{r}\,\frac{\phi_i(\mathbf{r})}{N_i}\ln\phi_i(\mathbf{r}) - \frac{1}{2\beta}\sum_i\int d\mathbf{r}\,\frac{1}{N_i\bar{\phi}_i}\{\delta\phi_i(\mathbf{r})\}^2 + \frac{1}{2\beta}\sum_{ij}\int d\mathbf{q}\, S_{ij}^{-1}(\mathbf{q})\,\delta\phi_i(\mathbf{q})\,\delta\phi_j(-\mathbf{q}) \tag{5}$$

where N_i is the length of the *i*th subchains (the superscript *p* is suppressed for simplicity). In eq 5, the first term is the Flory−Huggins mixing entropy of the centers of mass of the subchains. When this mixing entropy is expanded in a power series in $\delta\phi_i(\mathbf{r})$, the second-order term is given by the second term of eq 5. By subtracting this contribution and instead adding the more accurate expression, i.e., the third term that contains $S_{ij}^{-1}(\mathbf{q})$, one can generalize the Flory−Huggins free energy to inhomogeneous systems. In this model, it is essentially important in simulating the strong segregated systems that we retain the higher-order contributions in the expansion of the free energy. In eq 5, we can neglect the constant term and the terms linear in $\delta\phi_i(\mathbf{r})$ because these terms do not affect the phase separation dynamics. Thus, the second-order terms are the leading nontrivial contributions in the GL expansion.

Uneyama and Doi have simplified the third term of eq 5 by using the approximate form of the scattering function proposed by Ohta and Kawasaki[25] as $S_{ij}^{-1}(\mathbf{q}) = A_{ij}/\mathbf{q}^2 + B_{ij} + C_{ij}\mathbf{q}^2$, where A_{ij}, B_{ij}, and C_{ij} are fitting parameters. In addition to this simplification, Uneyama and Doi introduced another modification to eq 5. They introduced the essence of the Flory−Huggins−de Gennes theory by assuming the coefficient of the square gradient term $(\nabla\phi_i(\mathbf{r}))^2$ (i.e., the coefficient C_{ij} in the above approximated form) to be dependent on the local segment densities as $C_{ij} = \delta_{ij}b^2/\{24\phi_i(\mathbf{r})\}$. This modification is empirically known to be efficient in introducing the effects of the inhomogeneity in the segment density distribution into the model (mainly the effects of the inhomogeneity in the higher-order terms in the GL expansion). On the other hand, the inhomogeneity in our model will be treated by combining this PDF free energy with the exact SCF theory. Thus, we decided to use the original form of the $S_{ij}^{-1}(\mathbf{q})$ obtained using the RPA[22] without the empirical modification by Uneyama and Doi.

To obtain the exact expression of $S_{ij}^{-1}(\mathbf{q})$, the linear relation $u_i(\mathbf{q}) = \sum_j S_{ij}^{-1}(\mathbf{q})\,\delta\phi_j(\mathbf{q})$ is assumed in the RPA, where $\{u_i(\mathbf{r})\}$ is the external potential field and $S_{ij}^{-1}(\mathbf{q})$ is the *ij* element of the inverse matrix of the scattering function matrix of segment density fluctuations. Because of the incompressibility condition, one of the elements of $\{\delta\phi_i\}$ is not independent of the other. This leads to the use of a reduced scattering function matrix $\{\tilde{S}_{ij}^{-1}(\mathbf{q})\}$ instead of $\{S_{ij}^{-1}(\mathbf{q})\}$ itself. The details of the derivation of this scattering function matrix are given in Appendix A.

With this $\{\tilde{S}_{ij}^{-1}(\mathbf{q})\}$, we can explicitly calculate $\{u_i(\mathbf{r})\}$ without relying on any recursive calculations when the segment density distribution $\{\delta\phi_i(\mathbf{r})\}$ is given.

2.1.2. Free Energy and Chemical Potential. By using $\{\tilde{S}_{ij}^{-1}(\mathbf{q})\}$, the free energy of the system, eq 5, is rewritten as

$$\mathcal{F}[\{\phi_i(\mathbf{r})\}] = \frac{1}{\beta}\sum_i^n \int d\mathbf{r}\, \frac{\phi_i(\mathbf{r})}{N_i} \ln \phi_i(\mathbf{r}) - \frac{1}{2\beta}\sum_i^n \int d\mathbf{r}\, \frac{1}{N_i \bar{\phi}_i}\{\delta\phi_i(\mathbf{r})\}^2 + \sum_i^n \int d\mathbf{r}\, u_i(\mathbf{r})\, \delta\phi_i(\mathbf{r}) \quad (6)$$

The coefficients $\{u_i(\mathbf{r})\}$ in the third term of eq 6 are calculated by using the matrix $\{\tilde{S}_{ij}^{-1}\}$.

Using the free energy model eq 6, the chemical potential of the segments of the ith subchain is given by

$$\tilde{\mu}_i(\mathbf{r}) = \frac{\delta\mathcal{F}[\{\phi_i(\mathbf{r})\}]}{\delta\phi_i(\mathbf{r})} \quad (7)$$

$$= \frac{1}{\beta}\left\{\frac{\ln \phi_i(\mathbf{r})}{N_i} + \frac{1}{N_i} - \frac{1}{\bar{\phi}_i N_i}\delta\phi_i(\mathbf{r}) - \frac{\ln \phi_n(\mathbf{r})}{N_n} - \frac{1}{N_n} + \frac{1}{\bar{\phi}_n N_n}\delta\phi_n(\mathbf{r})\right\} + u_i(\mathbf{r}) \quad (8)$$

where the incompressibility condition is used. Under such an incompressibility condition, the nth elements $\phi_n(\mathbf{r})$ and $\delta\phi_n(\mathbf{r})$ are treated as dependent variables as

$$\phi_n(\mathbf{r}) = 1 - \sum_i^{n-1}\phi_i(\mathbf{r}) \quad (9)$$

$$\delta\phi_n(\mathbf{r}) = -\sum_i^{n-1}\delta\phi_i(\mathbf{r}) \quad (10)$$

These nth elements and $\tilde{\mu}_n(\mathbf{r})$ are not explicitly used in the dynamic calculations.

2.2. Dynamic Density Functional Theory. The time evolution equation for the segment density of the ith subchain can be described in terms of the chemical potential $\tilde{\mu}_i(\mathbf{r})$ under the assumption of Fick's law of linear diffusion for the segment densities as follows

$$\frac{\partial}{\partial t}\phi_i(\mathbf{r},t) = \nabla\cdot[L_i(\mathbf{r},t)\nabla\{\tilde{\mu}_i(\mathbf{r},t) + \lambda(\mathbf{r},t)\}] \quad (11)$$

where t is the time, $L_i(\mathbf{r},t)$ is the mobility of the segment of the ith subchain at position $\mathbf{r}$ at time t, and $\lambda(\mathbf{r},t)$ is the Lagrange multiplier determined by the local incompressible condition. The explicit expression of $\nabla\lambda(\mathbf{r},t)$ in eq 11 is given by

$$\nabla\lambda(\mathbf{r},t) = -\frac{\sum_i L_i(\mathbf{r},t)\, \nabla\mu_i(\mathbf{r},t)}{\sum_i L_i(\mathbf{r},t)} \quad (12)$$

The details are given in Appendix B.

We use the following density-dependent mobility

$$L_i(\mathbf{r},t) = L_i^0\phi_i(\mathbf{r},t) \quad (13)$$

where L_i^0 is a constant value. This assumption prevents the segment density $\phi_i(\mathbf{r},t)$ from being negative value. It is useful because the Taylor series expansion in terms of the density fluctuation $\delta\phi_i(\mathbf{r},t)$ around $\bar{\phi}_i$ does not guarantee the positiveness of the values of $\phi_i(\mathbf{r},t)$.

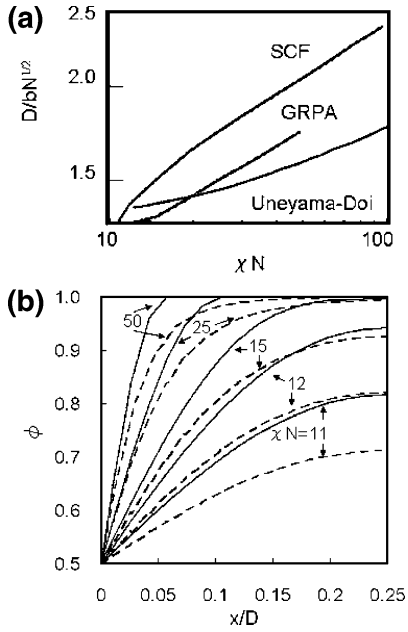

Figure 2. Results of an one-dimensional GRPA calculation on a symmetric AB diblock copolymer. (a) The simulation results of the SCF, GRPA, and Uneyam and Doi's theories[25] on the equilibrium periods D of the lamellar structure are shown for various values of the χN. (b) A comparison between the segment density profiles of the GRPA theory (solid lines) and those of the SCF theory (dashed lines) for the lamellar structure is shown.

A variable time mesh technique, whose detaila are described in Appendix C, is also adopted to avoid the negative values of the segment density $\phi_i(\mathbf{r},t)$.

2.3. Accuracy of the Dynamic GRPA Theory. We compare the domain structures of several block copolymer systems obtained using the dynamic GRPA theory with those obtained using some other theories.

2.3.1. One-Dimensional Lamellar Structure of a Symmetric Diblock Copolymer. Figure 2 shows the simulation results on the lamellar structure of a symmetric AB diblock copolymer (block ratio $f = 0.5$) melt obtained with the dynamic GRPA theory. The size of the simulation box is optimized using the dynamic system size optimization (SSO) method,[29] where the GRPA free energy is used in determining the rate of change of each side length of the simulation box.

Figure 2a shows the equilibrium period of the lamellar structure as a function of χN, where N is the total number of segments composing the block copolymer chain. The result of our GRPA theory lies between that of the SCF theory and that of Uneyama and Doi's theory. Both our GRPA theory and the Uneyama and Doi theory are based on the same GL expansion of the free energy and the RPA. The difference between these two theories comes from the use of the approximate form of the scattering function and the use of the local density-dependent coefficient of the square gradient term in Uneyama and Doi's theory. As the GRPA free energy coincides with the SCF free energy up to the second order in its Taylor series expansion, the behavior of the GRPA and SCF theories should be the same when the system approaches the critical point. We can actually confirm this in Figure 2a; i.e., the results of the GRPA and the SCF theories converge to the same result near the theoretical critical point ($\chi N = 10.5$ for symmetric block copolymer).

Figure 2b shows the profiles of the segment densities at the A/B interface of the lamellar structures shown in Figure 2a for different values of χN obtained by using GRPA and SCF theories. The interfacial profiles obtained with the GRPA theory

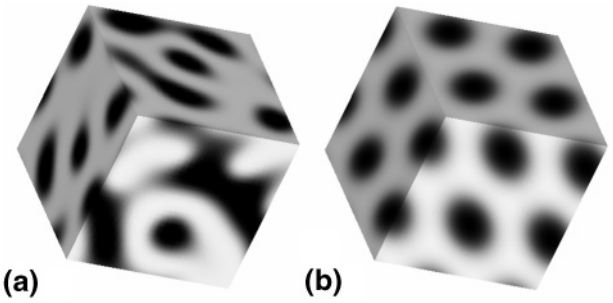

Figure 3. A comparison of the domain structures of a melt of an AB diblock copolymer with $N = 20$, $f = 0.35$, and $\chi N = 15$ calculated with the dynamic GRPA and the hybrid theories in the late stage is given. The spatial mesh size is 32^3 with the mesh width $\Delta x = 0.5375$. The values of f and χN correspond to those in the stable region of the hexagonally packed cylinder (HEX) structure on the phase diagram of the SCF calculation.[31]

are always sharper than those obtained with the SCF theory. The kinks of curves of GRPA for large values of χN are caused by the spatial discretization of the continuum segment densities. The origin of such a sharp interfacial profile is expected to be the approximate form of the higher-order terms in the expansion of the GRPA free energy where the effects of the chain conformation are neglected. The available region of the GRPA calculation extends up to about $\chi N = 50$, at which point the interfacial profile becomes too sharp to be simulated with a reasonable mesh size compared to that of the dynamic SCF theory.

2.3.2. Three-Dimensional Cylindrical Structure of a Diblock Copolymer. We tested the GRPA theory using a block copolymer system with a set of parameters which corresponds to the hexagonally packed cylinder (HEX) as the equilibrium state.[30,31] Figure 3 shows the comparison of the obtained structures between the dynamic GRPA theory (Figure 3a) and the dynamic SCF (Figure 3b) theory. The dynamic GRPA theory cannot reach the equilibrium HEX structure, while the dynamic SCF theory can. Such a discrepancy is caused by the difference of the free energy model between these two theories. The structure shown in Figure 3a has many 3-fold junctions, which are characteristic of the bicontinuous double gyroid (G) structure. We compared the densities of the GRPA free energy for the HEX structure (Figure 3b) and for the G structure[29] at this parameter set ($f = 0.35$ and $\chi N = 15$). This comparison showed that the G structure is more stable than the HEX structure for the GRPA model. This is due to the fact that the phase diagrams of diblock copolymers are quantitatively different between the SCF and GRPA theories. Thus, the GRPA theory cannot be used for quantitative evaluations of the phase diagram while the SCF theory can.

2.4. Hybrid Dynamic Density Functional Theory. The discrepancy between the GRPA and SCF theories as described in the preceding section is caused by the assumption in the evaluation of the higher-order terms in the Taylor series expansion in the GRPA theory. This is because the accuracy of the evaluated higher-order terms is depended on the treatment of the conformational entropy of the chains. The GRPA theory neglects the conformation entropy in the higher-order terms while the SCF theory evaluates them correctly.

To improve the accuracy of the dynamic GRPA theory up to the level of the dynamic SCF theory, one can combine these two theories. This can be achieved by adding a correction term $\Delta\bar{\mu}(\mathbf{r})$ to the chemical potential of the GRPA theory $\tilde{\mu}_i^{\mathrm{RPA}}(\mathbf{r},t)$ given in eq 8 as

$$\tilde{\mu}_i^{\mathrm{HYB}}(\mathbf{r},t) = \tilde{\mu}_i^{\mathrm{RPA}}(\mathbf{r},t) + \Delta\bar{\mu}_i(\mathbf{r},t) \tag{14}$$

where the $\tilde{\mu}_i^{\mathrm{HYB}}(\mathbf{r},t)$ means a corrected chemical potential. The correction term $\Delta\bar{\mu}_i(\mathbf{r})$ is defined as the difference between the chemical potential obtained with the SCF theory $\tilde{\mu}_i^{\mathrm{SCF}}(\mathbf{r},t)$ and that obtained with the GRPA theory $\tilde{\mu}_i^{\mathrm{RPA}}(\mathbf{r},t)$. Here we evaluate $\Delta\bar{\mu}_i(\mathbf{r})$ at every constant intervals of time t_{H} as

$$\Delta\bar{\mu}_i(\mathbf{r},t) = \tilde{\mu}_i^{\mathrm{SCF}}(\mathbf{r},nt_{\mathrm{H}}) - \tilde{\mu}_i^{\mathrm{RPA}}(\mathbf{r},nt_{\mathrm{H}}) \quad \text{for} \quad nt_{\mathrm{H}} \le t \le (n+1)t_{\mathrm{H}} \tag{15}$$

where n is a positive integer. This correction procedure hybridizes the dynamic SCF and dynamic GRPA theories.

Using this corrected chemical potential $\tilde{\mu}_i^{\mathrm{HYB}}(\mathbf{r},t)$, we can perform dynamic simulations. Although the speed of the calculation of the hybrid theory is slower than that of the dynamic GRPA theory, it is much faster than that of the dynamic SCF theory. The hybrid theory guarantees that the final equilibrium structure (or the steady state in the late stage) is the same as that produced in the late stage of the corresponding dynamic SCF simulation. If we choose the interval of the update of $\Delta\bar{\mu}_i(\mathbf{r})$ short enough, the result of the hybrid theory should trace that of the dynamic SCF theory. Therefore, the interval of update t_{H} is a crucial parameter for the accuracy of the hybrid theory. In practical calculations, the simulation time step is discretized with Δt. Thus, the number of time steps between the consecutive updates of $\Delta\bar{\mu}_i(\mathbf{r})$ is denoted by $n_{\mathrm{H}} = t_{\mathrm{H}}/\Delta t$. Hereafter, we will use this n_{H} to indicate the degree of the hybridization.

3. Simulation Results

In this section, we will test the accuracy and the efficiency of the hybrid theory by comparing its results with those of the dynamic GRPA and dynamic SCF theories using several examples.

In section 3.1, we check the quantitative accuracy of the hybrid theory by comparing the time dependences of the scattering function for various values of n_{H} using a two-dimensional symmetric A/B polymer blend that undergoes spinodal decomposition as a target system. We will see that the hybrid theory with a rather large value of n_{H} can reproduce the results of the correct SCF simulation well.

If one wants to obtain a qualitative (not quantitative) phase diagram of a given polymer system, a correct evaluation of the relative order of the values of the free energy for different microdomain structures is important. In section 3.2, we evaluate the free energy of a three-dimensional cylindrical structure of an asymmetric A−B diblock copolymer using both the GRPA and the SCF theories and compare their results to show that these two theories give qualitatively the same results.

The accuracy and the efficiency of the hybrid theory are expected to be strongly dependent on the choice of the correction interval n_{H}. We check such an effect in section 3.3. We will confirm that the hybrid theory is efficient and correct even with a large value of n_{H}. However, the hybrid theory is not always efficient. Such an exceptional example where the hybrid theory cannot trace the correct dynamics will be shown in section 3.4.

To show the usefulness of the hybrid theory, in section 3.5, we show results of the hybrid simulation on a formation of complex microphase-separated domains of a cast film of an ABC triblock copolymer where the microdomain structures are controlled dynamically through the evaporation of a selective solvent.[32,33]

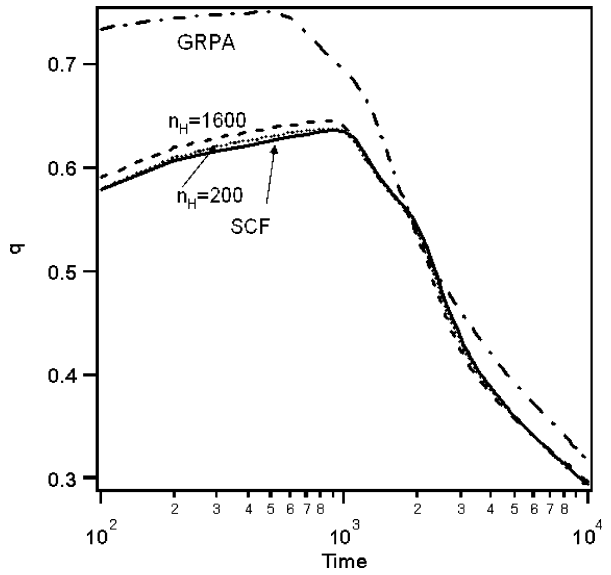

Figure 4. Time dependence of the wavenumber at the peak position of the scattering functions of an A/B polymer blend that undergoes spinodal decomposition is given. The system is a symmetric polymer blend with $N_A = N_B = 10$, $\bar{\phi}_A = \bar{\phi}_B = 0.5$, and $\chi N = 3$. The spatial mesh size is 256^2 with the spatial mesh width $\Delta x = 1.0$, and the time evolution is integrated with the time mesh width $\Delta t = 0.01$.

In all the simulations shown in this section, the effective bond lengths of all segments are assumed to be the same value b, which we use as the unit of length.

3.1. Quantitative Accuracy of the Hybrid Theory: A/B Polymer Blend Case. Here, we test the quantitative accuracy of the hybrid theory by using a two-dimensional A/B polymer blend system which undergoes a spinodal decomposition as an example. Figure 4 shows the time dependence of the wavenumber of the peak position of the circularly averaged scattering function. The wavenumber at the peak is obtained by fitting the scattering function by a Gaussian function using the least-squares method with 20 data points near the peak position (the range of $\mathbf{q}$ is $0.078b^{-1}$). The values of n_H are shown in the figure.

The time dependence of the peak position of the scattering function for the four cases with SCF ($n_H = 1$), hybrid ($n_H = 200$, 1600), and GRPA ($n_H = \infty$) are plotted in Figure 4. Here, the two curves for SCF and $n_H = 200$ are almost overlapping and the curve for $n_H = 1600$ is also very close to these curves. There is a tendency that the wavenumber of the dynamic GRPA theory is larger than that of the dynamic SCF theory; i.e., the GRPA theory underestimates the domain size than the SCF theory. This feature is the same as the one-dimensional calculation result of lamellar as shown in Figure 2a. On the other hand, it is surprising that the wavenumber of the hybrid theory with even a large value of n_H; i.e., $n_H = 1600$ coincides well with that of the dynamic SCF theory. This result demonstrates that the hybrid theory can trace the same morphological change of domains as the dynamic SCF theory. A further increase in n_H such as 3600 prevents the SCF iteration scheme from converging because the interfaces become too sharp in the late stage of the dynamic GRPA simulation.

3.2. Qualitative Accuracy of the Phase Behavior: Hexagonally Packed Cylinder Case. For a qualitative understanding of the phase behavior of a given system, it is essential that the theory can give correct order of the values of the free energy for different microdomain structures. Here, we check whether the GRPA theory can give a qualitatively the same result as the SCF theory which is regarded as a correct reference value. For this purpose, we perform hybrid simulations with different

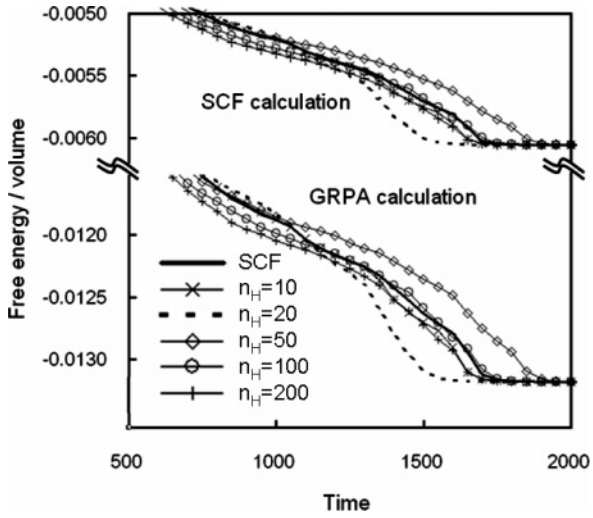

Figure 5. Time dependence of the free energy densities for the microphase separation of an AB diblock copolymer melt is shown. The simulation condition is the same as that of the system shown in Figure 3. Shown are the results of the hybrid calculations with several values of n_H with $\Delta t = 0.01$. The free energy density is evaluated with both the SCF (upper set of curves) and GRPA (lower set of curves) theories to show that these two theories give qualitatively the same results.

n_H values on the formation process of the HEX structure shown in Figure 3b, starting from an initial disordered state. For each simulation run, we evaluate the free energy based on the calculated segment density fields.

Figure 5 shows the time dependence of the free energy density for various values of n_H. The upper set of curves shows the free energy densities evaluated with the SCF theory while the lower set of curves shows those evaluated with the GRPA theory. In both sets, the segment density distributions are calculated with the hybrid theory with the n_H values shown in the figure. In all cases, the free energy converges to the same value in the late stage when the system reaches the equilibrium HEX phase, as shown in Figure 3b. Although the absolute values of the free energy are different for the two cases, i.e., SCF and GRPA theories, the overall and relative behaviors of the individual runs are almost the same for these two sets of curves. This result means that the computationally economical GRPA theory can be used in evaluating the free energy instead of the computationally expensive SCF theory as long as the dynamics is traced using the hybrid simulation method. Thus, a combination of the hybrid dynamical simulations and the free energy evaluation using GRPA theory is a useful technique to predict the (qualitative) nonequilibrium phase diagram. (Or we should call it as "stability diagram" because the system is not in the equilibrium state even in the final stage.)

3.3. Computational Efficiency of the Hybrid Theory. Figure 6 shows the relation between the n_H and the computational time required for the hybrid simulation. Here, the computational time is normalized with that of the dynamic SCF theory. Results for three different systems are shown: a one-dimensional symmetric A−B diblock copolymer melt in the lamellar phase, a two-dimensional symmetric A/B polymer blend which undergoes a spinodal decomposition (the same system as was shown in Figure 4), and a three-dimensional asymmetric A−B diblock copolymer melt in the HEX phase (the same as that shown in Figures 3 and 5).

The required computational time decreases with increasing n_H. This is not trivial because increasing n_H in general results in a larger difference between the GRPA result and the correct SCF result after n_H time steps, which leads to an increased

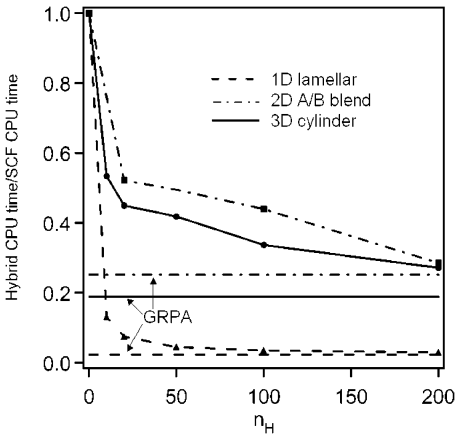

Figure 6. Dependence of the performance of the hybrid theory on the model parameters and the used techniques is shown. The computational times for individual runs are normalized using that for the full SCF calculation ($n_H = 1$). Results for three types of simulations with $\Delta t = 0.01$ are indicated: (a) a one-dimensional diblock copolymer system with $N = 100$, $f = 0.5$, $\chi N = 15$, and the number of grid points = 64 with mesh width $\Delta x = 0.25$; (b) a two-dimensional A/B polymer blend system whose simulation condition is the same as that in Figure 4; and (c) a three-dimensional diblock copolymer system whose simulation condition is the same as that in Figure 3. The horizontal lines indicate the necessary computational time for the dynamic GRPA theory, which gives the lower limit of the hybrid simulations.

number of iterations in the SCF calculation. The reduction rate depends on the simulation conditions, i.e., the system size, the number of components, and the molecular architecture of the polymers. In the same figure, the computational times required for the dynamic GRPA simulations ($n_H = \infty$) are also shown with the horizontal lines, which give the lower limits for the computational times for the hybrid theory. These results show that the computational efficiency of the hybrid theory quickly approaches its optimum value (the GRPA case) when the value of n_H is larger than a critical value.

3.4. Inefficient Case for the Hybrid Theory. There are certain systems where a very small value of n_H ($n_H \sim 5$) is required for the hybrid theory to trace the result of the dynamic SCF theory. Such an inefficiency is caused by the discrepancy between the equilibrium segment density profiles calculated with the GRPA and the SCF theories.

As an example, Figure 7 shows the one-dimensional segment density profiles of a blend of an ABA triblock copolymer and a B homopolymer. Figure 7a is the profile obtained with the dynamic GRPA theory, while Figure 7b is that obtained with the SCF theory. In Figure 7a, an accumulation of the A segments and the B segments of the ABA copolymer is observed at the interfaces between the domains of the B segments of the B homopolymer. There is no internal fine structure in such interfacial regions. On the other hand, in Figure 7b, one can observe a microphase separation of the A segments and the B segments of the ABA copolymer inside these interfacial regions. Such a discrepancy means that the GRPA theory cannot reproduce the fine structure in the interfacial region. Thus, in order for the hybrid theory to trace the correct SCF results, one has to use a small n_H to keep track of the change in the correct segment profile of the SCF theory at any time step of the dynamical simulations.

Even with a small value of n_H, the efficiency of the hybrid theory is still better than that of the full SCF theory ($n_H = 1$), as was discussed in Figure 6. Figure 8 shows a result of a hybrid simulation with $n_H = 5$ on the same system as was shown in Figure 7. The ABA copolymer forms micelles in the matrix of the B homopolymer. The micelles have the core−shell structure

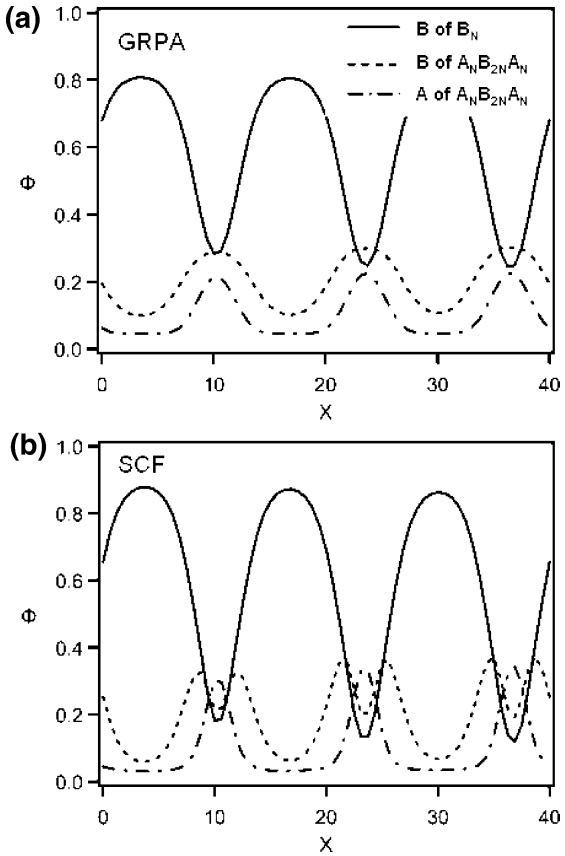

Figure 7. A comparison of the segment density profiles between the dynamic GRPA and dynamic SCF theories for an exceptional case that requires small n_H for the hybrid theory is given. The system is a one-dimensional polymer blend composed of a homopolymer B_N and a triblock copolymer $A_NB_{2N}A_N$ with $N = 10$, $\chi = 1.08$, and $\bar{\phi}_B = 0.6$. (a) The segment density profile obtained with the GRPA theory and (b) that obtained with the SCF theory are shown. In the latter case, a fine structure inside the interfacial region can be observed, which cannot be reproduced in the former case.

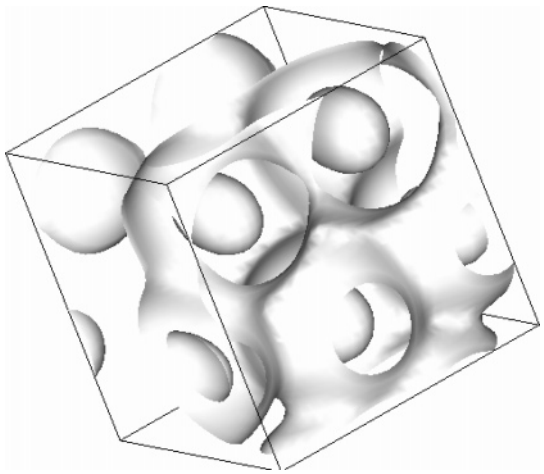

Figure 8. A domain structure of a three-dimensional $B_N/A_NB_{2N}A_N$ blend obtained with the hybrid theory with $n_H = 5$ at $t = 2000$ is shown. The condition of the system is the same as that of Figure 7. The simulation is done on a 3-dimensional mesh with 40^3 mesh points. The isosurfaces of the B segment density of the ABA copolymer at the value 0.2 are shown.

of which the core and shell are formed by the A and B segments of the ABA polymer, respectively. Such a complex domain structure can be obtained with the hybrid theory with a considerably improved efficiency compared to the SCF theory.

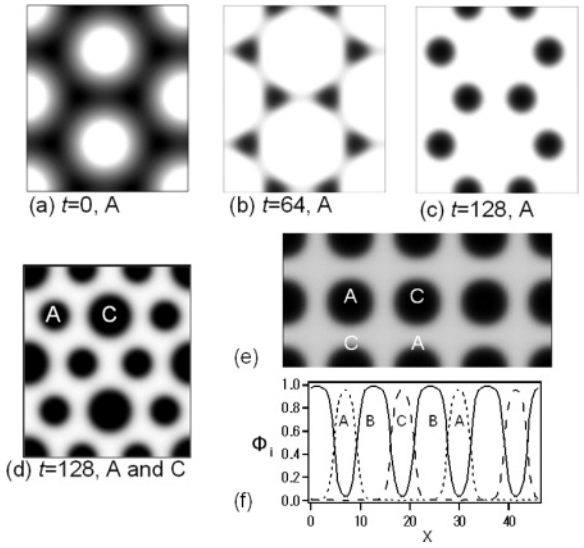

Figure 9. Time dependence of the formation of the domain structure of a melt of an $A_{20}B_{60}C_{20}$ polymer starting from an equilibrium HEX structure of the C segments is shown. (a) The initial distribution of A segments (black) where C segments form the HEX structure and, A and B segments form the matrix phase. The used parameters are $\chi_{AB} = 0$ and $\chi_{AC} = \chi_{BC} = 0.4$, and the system size is 30.5×35.2, which is divided into 64^2 meshes. In order to adjust the system size to the natural period of the HEX structure, we used the SSO method.[29] At $t = 0$ the χ parameters are suddenly changed to $\chi_{AB} = \chi_{AC} = \chi_{BC} = 0.4$. Then, the phase separation process is simulated with $n_H = 5$ (b and c). The A segment distributions at (b) $t = 64$ and (c) $t = 128$ are shown. (d) is the same system as in (c), but both the A and the C segments are shown simultaneously where the A segments form a spatial motif around the HEX structure of the C segment. (e) is the square-lattice cylinder structure obtained with the static SCF calculation with SSO using (d) as the initial condition. (f) is the segment density profile of the most stable lamellar structure. All figures are shown in the same scale with periodic boundary conditions.

3.5. Morphology of an ABC Triblock Copolymer Controlled by Solvent Selectivity. It is known that a cast film of polystyrene-*block*-polybutadiene-*block*-poly(methyl methacrylate) (SBM) solvated with a tetrahydrofuran (THF) solution often shows a structural motif, i.e., a characteristic microdomain formation. For example, in refs 32 and 33, a HEX structure of the triblock copolymer is controlled by changing the selectivity of the THF solvent to each of the blocks. In the process of the evaporation of the THF, HEX domains composed of the poly(methyl methacrylate) (PM) first appear, where the PS and PB blocks make a uniform matrix phase. After such HEX domains are formed, the PS segments start to accumulate around the HEX domains of PM and form a structural motif.

As is easily anticipated, the final structure is a nonequilibrium state which depends on the kinetic pathway that reaches this final state. Thus, we need a dynamical simulation that can take the complex structures of polymers and domains into account by correctly evaluating the free energy of the system. We simulated this phenomenon using a hybrid simulation on a two-dimensional ABC triblock copolymer system. We assume that the SBM triblock copolymer is modeled with an $A_{20}B_{60}C_{20}$ triblock copolymer. The evaporation of the THF solvent is effectively modeled as a change in the value of the χ_{ij} parameters. The simulation results are shown in Figure 9, where the segment densities of the A segments are shown. Figure 9a shows the initial HEX structure of the C segments obtained with SSO, where the χ parameters are chosen as $\chi_{AB} = 0.0$ and $\chi_{AC} = \chi_{BC} = 0.4$. In this initial state, the A and B segments are dissolved in the THF solvent to form a matrix. Starting from this initial HEX structure, a domain formation of the A (PS) segments is simulated by changing the χ parameters to $\chi_{AB} = \chi_{AC} = \chi_{BC} = 0.4$, which corresponds to a change in the quality of the THF solvent by a solvent evaporation. In this simulation, we assumed that the system size is not changed because the solvent has evaporated already in the initial state, which means that the system size cannot change.

It is true that this method of simulating the solvent evaporation is a phenomenologically conventional way, as was pointed out in ref 34. We decided, however, to adopt this conventional method because the realistic treatment discussed in ref 34 is beyond the scope of this article. (We could perform more realistic simulations by introducing the degrees of freedom of the solvent directly, which is a target of the future publications.) Instead, we will present the simulation results on the ABC triblock copolymer as one of the typical examples of complex systems for which the hybrid approach gives reasonable results with an improved efficiency.

Parts b and c of Figure 9 show the time-dependent distributions of the A segments. The A segments migrate in the matrix as Figure 9b and make a hexagonally arranged structural motif, as shown in Figure 9c. To show the fine structure of the system in Figure 9c, we show in Figure 9d the same system as in Figure 9c but show the final segment density profiles of both the A and the C segments. We can confirm that the system is composed of a HEX domains of the C segments surrounded by the motif of the A segments.[32,33]

It is important to note that this motif structure is a metastable structure that can be realized in the nonequilibrium dynamic domain formation process. Because the $A_{20}B_{60}C_{20}$ triblock copolymer with $\chi_{ij} = 0.4$ for all pairs of different segment types is symmetric with respect to the exchange of A and C, the equilibrium structure should also have the same symmetry. One of such symmetric structures is a square lattice as shown in Figure 9e where cylinders composed of A and C segments are placed alternatively on a square lattice.[35] This square lattice structure is obtained with the static SCF calculation with SSO starting from the structure shown in Figure 9d as the initial condition. This condition corresponds to the annealing process where the system size can change according to the strain of the domain structure.

Another candidate of the equilibrium structure is the symmetric lamellar structure with the arrangement of the domains as ABCBA... (shown in Figure 9f), which is also obtained with the static SCF theory with SSO starting from a uniform initial condition.

We evaluated the free energy density for the above-mentioned three structures, i.e., the motif structure, the square lattice structure, and the lamellar structure, and we found that

$$F_{\text{lamellar}} < F_{\text{square lattice}} < F_{\text{motif}}$$

Thus, the true equilibrium structure is neither the motif structure nor the square-lattice structure but the lamellar structure. This result demonstrates the usefulness of the hybrid theory, which can reproduce a dynamic and complex domain formation process with a considerably improved calculation efficiency than the dynamic SCF theory.

4. Discussion

The GRPA theory is based on both the Flory−Huggins theory and the RPA up to the second-order terms in the series expansion of the free energy. These assumptions cause a deviation of the chemical potential from that of the SCF theory. Although the dynamic simulation based on the GRPA theory can follow the dynamic SCF calculation qualitatively as shown in Figure 4,

the result of the GRPA theory is quantitatively inadequate. The hybrid theory can correct this deviation and reproduces the result of the SCF theory as shown in Figures 4 and 5.

Our GRPA theory uses the same free energy model of Bohbot-Raviv and Wang's theory,[24] where we use the exact expressions of the scattering functions derived using the RPA, while Ohta-Kawasaki[23] and Uneyama and Doi's[25] theories use approximate expressions of the scattering functions. While Bohbot-Raviv and Wang reported the results only for static and two-dimensional systems, we performed three-dimensional dynamic calculation for polymer melts and blends of any polymer architectures using our GRPA theory.

Uneyama and Doi have reported that Bohbot-Raviv and Wang's theory cannot give the correct dependence of the interfacial tension of a block copolymer melt on its block ratio.[25] Moreover, both the dynamic GRPA theory and the Uneyama and Doi theory show a considerable deviation from the result of the SCF theory as shown in Figure 2a, especially in the strong segregation region. These difficulties are eliminated with the use of the hybrid theory.

In the GRPA theory, the coefficients of the series expansion of the free energy are calculated in the Fourier space. Thus, the use of the GRPA theory is limited to the systems with proper boundary conditions that are adapted to the Fourier transformation. This condition makes it difficult to apply the dynamic GRPA and hybrid theories to the systems without periodic boundary conditions, such as a system subjected to a solid wall.

As a result of the above discussions, we understand that the hybrid theory suffers from the limitations of both the dynamic SCF and the dynamic GRPA theories. The numerical scheme of the dynamic SCF theory is in general more robust than the dynamic GRPA theory. Thus, it is usually enough for the hybrid theory to satisfy the standard condition for the dynamic SCF theory. The most severe restriction on the GRPA theory is the fact that the system is limited within the weak segregation regime. However, such a limitation is released by the combination of the SCF and GRPA. Thus, the conditions for the hybrid theory to be valid are almost the same as those for the dynamic SCF theory.

5. Conclusion

We proposed a hybrid theory for the dynamics of the phase separation phenomena of polymer melts and blend systems composed of polymers with any molecular architectures. To improve the efficiency and accuracy, the dynamic SCF and dynamic GRPA theories are hybridized. The former is quantitatively accurate while the latter has an advantage in the computational efficiency. Although the parameters required for the GRPA theory are the same as those for the SCF theory, the GRPA theory demands neither the recursive calculations nor any extra model parameters such as the empirical parameters required for the GL free energy. In the hybrid theory, the time evolution of the segment density fields is mainly calculated using the chemical potential of the GRPA theory, which is corrected using the chemical potential of the SCF at some intervals.

We confirmed that this hybrid theory accelerates the dynamic SCF theory without loss of its accuracy in a symmetric 1D A−B diblock copolymer, a symmetric 2D A/B polymer blend, and a 3D A−B diblock copolymer system whose equilibrium phase is the cylindrical phase. We also confirmed that the dynamic hybrid theory well reproduces the morphological changes of domains quantitatively in several systems. Therefore, we estimate that this hybrid theory will enable us to perform accurate large-scale simulations on polymer melts and blend systems.

Acknowledgment. The authors thank Prof. M. Doi (Tokyo University) and T. Uneyama (Kyoto University) for many comments and discussions. This study is executed under the national project on nanostructured polymeric materials, which has been entrusted to the Japan Chemical Innovation Institute by the New Energy and Industrial Technology Development Organization (NEDO) under METi's Program for the Scientific Technology Development for Industries that Create New Industries. This work is partially supported by the Grant-in-Aid for Science from the Ministry of Education, Culture, Sports, Science and Technology, Japan on the priority area "Soft Matter Physics".

Appendices

A. Scattering Functions Based on RPA for Polymers with Any Molecular Architectures. In this appendix, we derive an exact expression of the inverse of the scattering function matrix $\mathbf{S}^{-1}(\mathbf{q}) \equiv \{S_{ij}^{-1}(\mathbf{q})\}$. For the simplicity of the descriptions, we define vectors of the Fourier modes of the segment density fluctuations of each subcahin and the external potentials acting on each segment density as

$$\mathbf{x}(\mathbf{q}) \equiv \{\delta\phi_i(\mathbf{q})\} \tag{16}$$

$$\mathbf{u}(\mathbf{q}) \equiv \{u_i(\mathbf{q})\} \tag{17}$$

We also define the same vectors but in the real space as

$$\mathbf{x}(\mathbf{r}) \equiv \{\delta\phi_i(\mathbf{r})\} \tag{18}$$

$$\mathbf{u}(\mathbf{r}) \equiv \{u_i(\mathbf{r})\} \tag{19}$$

where $\mathbf{r}$ is the position vector. A linear relation $\mathbf{x}(\mathbf{q}) = \mathbf{S}(\mathbf{q})\,\mathbf{u}(\mathbf{q})$ between these two vectors is assumed, where the coefficient matrix $\mathbf{S}(\mathbf{q})$ corresponds to the inverse of $\mathbf{S}^{-1}(\mathbf{q})$. Because of the incompressibility condition, one of the elements of $\mathbf{x}$ is not independent of the other, and therefore $\mathbf{S}(\mathbf{q})$ is a singular matrix. Then, in order to obtain $\mathbf{S}^{-1}(\mathbf{q})$, we introduce $\tilde{\mathbf{S}}(\mathbf{q})$ where one of the rows and corresponding column of $\mathbf{S}(\mathbf{q})$ are eliminated so that $\tilde{\mathbf{S}}^{-1}(\mathbf{q})$ can exist.

We introduce a matrix whose elements are the scattering functions of ideal Gaussian chains as

$$\mathbf{S}^0 \equiv \{S_{ij}^0(\mathbf{q})\} \tag{20}$$

where $S_{ij}^0(\mathbf{q}) = 0$ if the ith and jth subchains belong to different polymers. The explicit expressions of the elements $S_{ij}^0(\mathbf{q})$ are given later. We also define a matrix of the segment interaction energy as

$$\mathbf{C} \equiv \{z\epsilon_{ij}\} \tag{21}$$

where ϵ_{ij} means the interaction energy between segments of the ith and jth subchains. Hereafter, the expressions $\mathbf{x}$ and $\mathbf{u}$ without arguments are only used for those in the Fourier space.

The incompressibility condition generates a static pressure that is common to all the subchains. We denote this static pressure in the Fourier space as $u^*(\mathbf{q})$. This u^* is a function of $\mathbf{u}$, $\mathbf{S}^0$, and $\mathbf{C}$ as

$$u^* = f(\mathbf{u}, \mathbf{S}^0, \mathbf{C}) \tag{22}$$

Using the quantities introduced above, the self-consistent equation is given by

$$\mathbf{x} = -\beta\mathbf{S}^0(\mathbf{u} + \mathbf{C}\mathbf{x} + u^*\mathbf{e}) \tag{23}$$

where **e** is the vector whose all elements are unity. This equation is the fundamental equation of the generalized RPA that gives the coefficient of the second-order term in the free energy expansion. According to Leibler, the sum of terms in parentheses on the right-hand side of eq 23 is called the effective potential that is an external potential renormalized by the internal interactions and the incompressibility condition.[22] Solving eq 23 with respect to **x** gives

$$\begin{aligned}\mathbf{x} &= -\beta(\mathbf{E} + \beta\mathbf{S}^0\mathbf{C})^{-1}\mathbf{S}^0(\mathbf{u} + u^*\mathbf{e}) \\ &= -\beta(\mathbf{B}\mathbf{u} + u^*\mathbf{B}\mathbf{e})\end{aligned} \tag{24}$$

where **E** is the identity matrix and $\mathbf{B} = (\mathbf{E} + \beta\mathbf{S}^0\mathbf{C})^{-1}\mathbf{S}^0$. Here the incompressibility condition must be satisfied for **x** as

$$\sum_{i=1}^{n} x_i = 0 \tag{25}$$

From eqs 24 and 25, u^* is obtained as

$$u^* = -\frac{\sum_{i=1}^{n}\sum_{j=1}^{n} B_{ij}u_j}{\sum_{i=1}^{n}\sum_{j=1}^{n} B_{ij}} \tag{26}$$

Substituting eq 26 into eq 24 leads to

$$\mathbf{x} = -\beta\mathbf{S}\mathbf{u} \tag{27}$$

where $\mathbf{S} = \mathbf{B} + \mathbf{B}'$ and the element of the matrix $\mathbf{B}'$ is defined as

$$B'_{ij} = -\frac{(\sum_{j'=1}^{n} B_{ij'})(\sum_{i'=1}^{n} B_{i'j})}{\sum_{i'=1}^{n}\sum_{j'=1}^{n} B_{i'j'}} \tag{28}$$

If the inverse of **S** can be obtained in eq 27, we can get $\mathbf{u} = (-1/\beta)\mathbf{S}^{-1}\mathbf{x}$, and this **u** can be used for the calculation of the free energy. However, because of the incompressibility condition, eq 25, the matrix **S** is a singular matrix; i.e., the rank of **S** is $n - 1$. This means that the segment densities of n subchains are not independent. Then, we take the segment densities of the subchains $i \leq n - 1$ as the independent variables and the segment density of the nth subchain as a dependent one. In this case, we should calculate the inverse matrix of the $(n - 1) \times (n - 1)$ block in the upper left part of **S**. Then, we define an $n \times n$ matrix $\tilde{\mathbf{S}}^{-1}$, where the $(n - 1) \times (n - 1)$ block in the upper left part is filled with the inverse matrix obtained above and the nth row and column are filled with 0 elements.

By using the $\tilde{\mathbf{S}}^{-1}$, the **u** is given by

$$\mathbf{u} = -\frac{1}{\beta}\tilde{\mathbf{S}}^{-1}\mathbf{x} \tag{29}$$

The $\tilde{\mathbf{S}}^{-1}$ in eq 29 is the exact and general expression of the inverse scattering function derived with the RPA. It should be noted that the matrix $\tilde{\mathbf{S}}^{-1}$ is time independent for the canonical ensemble system. Therefore, in practical calculation, there is no need to update the $\tilde{\mathbf{S}}^{-1}$ for each time step of the dynamical simulations.

A.1. Subchain Scattering Function Matrix. We denote the indices of the subchains in the p-type polymer by i' and j'. Then the scattering function from the p-type polymer which is assumed to be an ideal Gaussian chain is given by

$$S^{0p}_{i'i'}(\mathbf{q}) = \frac{1}{N^p}\int_0^{N_{i'}(p)} ds \int_0^{N_{i'}(p)} ds' \exp\left(-\frac{\mathbf{q}^2}{6}\left|s - s'\right|b^2\right) = \frac{2N_{i'}^{(p)}}{N^{(p)}x^2}(e^{-x} - 1 + x) \tag{30}$$

$$S^{0p}_{i'j'}(\mathbf{q}) = \frac{1}{N^{(p)}}\int_0^{N_{i'}(p)} ds \int_0^{N_{i'}(p)} ds' \exp\left(-\frac{\mathbf{q}^2}{6}\left|s - s'\right|b^2\right) = \frac{N_{i'}^{(p)}\,N_{j'}^{(p)}e^{-z}}{N^{(p)}xy}(e^{-x} - 1)(e^{-y} - 1) \quad (i' \neq j') \tag{31}$$

where x, y, and z are given by

$$x \equiv R_{Gi'}{}^2|\mathbf{q}|^2, \quad y \equiv R_{Gj'}{}^2|\mathbf{q}|^2, \quad \text{and} \quad z \equiv R_{Gi'j'}{}^2|\mathbf{q}|^2 \tag{32}$$

$R_{Gi'}$ and $R_{Gj'}$ are the radii of gyration ($R_G = (1/6)Nb^2$) of the i'th and j'th subchains, respectively, and $R_{Gi'j'}$ is the radius of gyration of a sequence of subchains that connects the i'th and j'th subchains.

As a result, the explicit expression of the $S^0_{ij}(\mathbf{q})$ is obtained as a product of the average volume fraction of the p-type polymer in the system $\bar{\phi}_p$ and the $S^{0p}_{i'j'}(\mathbf{q})$ as

$$S^0_{ij}(\mathbf{q}) = \bar{\phi}_p S^{0p}_{i'j'}(\mathbf{q}) \tag{33}$$

$$i = \sum_{p'}^{p-1} n^{(p')} + i' \tag{34}$$

where $\mathbf{S}^0$ is a symmetric matrix that satisfies $S^0_{ij}(\mathbf{q}) = S^0_{ji}(\mathbf{q})$ and the diagonal element $S^0_{ii}(\mathbf{q})$ is the self-scattering function of the ith subchain. The subscript index i for subchains in the system is expressed by using the subscript index i' for subchains in the polymer as eq 34.

B. The Treatment of the Incompressibility Condition in the Equation of Motion. Under the incompressibility condition, the free energy $\mathscr{F}[\{\phi_i(\mathbf{r},t)\}]$ is modified as

$$\mathscr{F}'[\{\phi_i(\mathbf{r},t)\}] = \mathscr{F}[\{\phi_i(\mathbf{r},t)\}] + \int d\mathbf{r}\, \lambda(\mathbf{r},t)[\sum_i \phi_i(\mathbf{r},t) - 1] \tag{35}$$

where the $\lambda(\mathbf{r},t)$ is the Lagrange multiplier of the incompressibility condition. Substituting this equation into the time evolution equation for the segment density gives

$$\frac{\partial}{\partial t}\phi_i(\mathbf{r},t) = \nabla\cdot\left[L_i(\mathbf{r},t)\nabla\left\{\frac{\delta\mathscr{F}'[\{\phi_i(\mathbf{r},t)\}]}{\delta\phi_i(\mathbf{r},t)}\right\}\right] \tag{36}$$

$$= \nabla\cdot[L_i(\mathbf{r},t)\nabla\{\tilde{\mu}_i(\mathbf{r},t) + \lambda(\mathbf{r},t)\}] \tag{37}$$

The incompressibility condition demands

$$\frac{\partial}{\partial t}\sum_i \phi_i(\mathbf{r},t) = 0 \tag{38}$$

Thus

$$\nabla\cdot[\sum_i L_i(\mathbf{r},t)\nabla\tilde{\mu}_i(\mathbf{r},t) + \sum_i L_i(\mathbf{r},t)\nabla\lambda(\mathbf{r},t)] = 0 \tag{39}$$

This equation leads to

$$\sum_i L_i(\mathbf{r},t)\nabla\lambda(\mathbf{r},t) = -\sum_i L_i(\mathbf{r},t)\nabla\tilde{\mu}_i(\mathbf{r},t) + \mathbf{A} \tag{40}$$

where **A** is an integration constant. This vector **A** physically means a constant flux flowing throughout the system such as a flux imposing the boundary conditions. Thus, in the present situation, this constant flux **A** can be assumed to vanish. Solving eq 40 with respect to $\nabla\lambda(\mathbf{r},t)$ gives eq 12.

C. Variable Time Mesh Technique for the Dynamic Density Functional Theory. We introduce a dynamic density functional technique, which is basically a technique for the minimization of the free energy. Therefore, when we use the dynamic simulation for the purpose of searching for the local equilibrium structure, a faster convergence is desirable because we do not concern the actual time evolution of the system. For this purpose, we propose an algorithm for the acceleration of the dynamic density functional theory as follows.

We set the initial time step width Δt for a simulation and then introduce a time step ratio r_t ($r_t > 1$) and the upper limit of the time step width Δt_{max} which is now treated as a variable. Then, we modify the time step width Δt according to the following algorithm:

(1) Set the initial Δt.

(2) Perform one-step calculation of the dynamics simulation.

(3) If some of the segment densities become negative, then return to the state just before the previous step (2) is performed. Then, change Δt as $\Delta t \leftarrow \Delta t/r_t$ and recalculate step (2). Otherwise, go to step (4).

(4) Change Δt as $\Delta t \leftarrow \Delta t r_t$. If Δt exceeds Δt_{max}, then $\Delta t \leftarrow \Delta t_{max}$.

(5) Increase the time of the simulation system by Δt and go to step (2).

This acceleration technique becomes effective for a structural change of a system in its early stage and also in the very late stage after the system almost reaches the equilibrium structure. A large Δt is automatically chosen for such early and very late stages.

For the purpose of a rough estimation of the equilibrium structure, this acceleration technique combined with the dynamic GRPA theory is useful and efficient compared to the full dynamic SCF theory because the SCF theory demands many iterations for a large Δt value.

References and Notes

(1) Paul, D. R.; Newman, S. *Polymer Blends*; Academic Press: New York, 1978.
(2) Utracki, L. A. *Polymer Alloys and Blends*; Carl Hanser: New York, 1990.
(3) Fleer, G. J.; Cohen Stuart, M. A.; Scheutjens, J. M. H. M.; Cosgrove, T.; Vincent, B. *Polymers at Interfaces*; Chapman & Hall: London, 1993.
(4) Fredrickson, G. H.; Ganesan, V.; Drollet, F. *Macromolecules* **2002**, *35*, 16−39.
(5) Matsen, M. W. *J. Phys.: Condens. Matter* **2002**, *14*, R21−R47.
(6) Kawakatsu, T. *Statistical Physics of Polymers*; Springer-Verlag: Berlin, 2004.
(7) Helfand, E.; Wasserman, Z. R. *Macromolecules* **1976**, *9*, 879−888. Helfand, E.; Wasserman, Z. R. *Macromolecules* **1978**, *11*, 960−966. Helfand, E.; Wasserman, Z. R. *Macromolecules* **1980**, *13*, 994−998.
(8) Hong, K. M.; Noolandi, J. *Macromolecules* **1981**, *14*, 727−736.
(9) Fraaije, J. G. E. M. *J. Chem. Phys.* **1993**, *99*, 9202−9212.
(10) Hasegawa, R.; Doi, M. *Macromolecules* **1997**, *30*, 5490−5493.
(11) Morita, H.; Kawakatsu, T.; Doi, M. *Macromolecules* **2002**, *117*, 8153−8161.
(12) Zvelindovsky, A. V.; Sevink, G. J. A.; van Vlimmeren, B. A. C.; Maurits, N. M.; Fraaije, J. G. E. M. *Phys. Rev. E* **1998**, *57*, R4879−R4882. Zvelindovsky, A. V.; Sevink, G. J. A.; Fraaije, J. G. E. M. *Phys. Rev. E* **2000**, *62*, R3063−R3066.
(13) de Gennes, P. G. *J. Chem. Phys.* **1980**, *72*, 4756−4763.
(14) Oono, Y.; Puri, S. *Phys. Rev. Lett.* **1987**, *58*, 836−839.
(15) Qi, S.; Wang, Z. G. *Phys. Rev. Lett.* **1996**, *76*, 1679−1682. Qi, S.; Wang, Z. G. *Phys. Rev. E* **1997**, *55*, 1682−1697. Qi, S.; Wang, Z. G. *Polymer* **1998**, *39*, 4639−4648.
(16) Kodama, H.; Doi, M. *Macromolecules* **1996**, *29*, 2652−2658.
(17) Nonomura, M.; Ohta, T. *J. Phys. Soc. Jpn.* **2001**, *70*, 927−930. Nonomura, M.; Ohta, T. *Physica A* **2002**, *304*, 77−84. Nonomura, M.; Ohta, T. *J. Phys.: Condens. Matter* **2003**, *15*, L423−L430.
(18) Yamada, K.; Nonomura, M.; Ohta, T. *Macromolecules* **2004**, *37*, 5762−5777.
(19) Ren, S. R.; Hamley, I. W. *Macromolecules* **2001**, *34*, 116−126.
(20) de Gennes, P. G. *J. Phys. (Paris)* **1970**, *31*, 235−238.
(21) de Gennes, P. G. *Scaling Concepts in Polymer Physics*; Cornell University Press: Ithaca, NY, 1979.
(22) Leibler, L. *Macromolecules* **1980**, *13*, 1602−1617.
(23) Ohta, T.; Kawasaki, K. *Macromolecules* **1986**, *19*, 2621−2632.
(24) Bohbot-Raviv, Y.; Wang, Z.-G. *Phys. Rev. Lett.* **2000**, *85*, 3428−3431.
(25) Uneyama, T.; Doi, M. *Macromolecules* **2005**, *38*, 196−205.
(26) Uneyama, T.; Doi, M. *Macromolecules* **2005**, *38*, 5817−5825.
(27) Uneyama, T.; Ohta, T. *Polym. Prepr., Jpn. Polym. Soc.* **2005**, *55*, 1Ph064.
(28) Honda, T.; Kodama, H.; Roan, J.-R.; Morita, H.; Urashita, S.; Hasegawa, R.; Yokomizo, K.; Kawakatsu, T.; Doi, M. *SUSHI Users Manual*; OCTA: Nagoya, Japan, 2004 (http://octa.jp).
(29) Honda, T.; Kawakatsu, T. *Macromolecules* **2006**, *39*, 2340−2349.
(30) Honda, T.; Kawakatsu, T. In *Nanostructured Soft Matter: Experiments, Theory and Perspectives*; Zvelindovsky, A., Ed.; Springer-Verlag, in press.
(31) Matsen, M. W.; Schick, M. *Phys. Rev. Lett.* **1994**, *72*, 2660−2663.
(32) Brinkmann, S.; Stadler, R.; Thomas, E. L. *Macromolecules* **1998**, *31*, 6566−6572.
(33) Abetz, V.; Markgraf, K.; Rebizant, V. *Macromol. Symp.* **2002**, *177*, 139−145.
(34) Naughton, J. R.; Matsen, M. W. *Macromolecules* **2002**, *35*, 5688−5696.
(35) Nakazawa, H.; Ohta, T. *Macromolecules* **1993**, *26*, 5503−5511.

MA0620464